

PULLOUT RESISTANCE OF LARGE GEOGRID SPECIMENS IN SITE SPECIFIC SOILS

G. E. Bauer¹ and Q. Shang²

SYNOPSIS

This experimental study investigates the anchorage capacity of soil-reinforcement systems which consisted of uniaxial polymer geogrids and various soils. Geogrid pullout tests were carried out in a large test assembly.

The pullout results of four soil-reinforcement systems subjected to three normal stress intensities are presented and discussed in relation to soil shear strength properties. The tensile force distribution in the embedded geogrid was estimated from elongation measurements along the geogrid.

The large pullout facility has given good results for estimating the anchorage capacity of soil-reinforcement systems and for verifying analytical concepts.

INTRODUCTION

Reinforced soil structures have undergone a rapid development and have been used in numerous geotechnical engineering applications. It has been suggested that the pullout test is a more realistic model of soil-reinforcement interaction than the sliding shear test (Ingold, 1983). The objective of the project was to conduct pullout tests on geogrids in site specific soils. The large test facility allowed the soil to be placed under controlled and site specific conditions and to minimize boundary effects generally associated with small apparatuses. This study was aimed to determine the anchorage capacity of soil-reinforcement systems, the soil-geogrid interface strength in relation to normal stress and the tensile force distribution in the embedded geogrid. A uniaxial geogrid (Tensar UX1600) was tested in different soils. Both granular and cohesive soils were used. The surcharge pressure ranged from 12 kPa to 21 kPa. These low normal stresses were governed by the long length of the grid adopted and the tensile strength of the geogrids. The geogrid specimens in contact with the soil had dimensions of 1.55 m in length by 0.73 m in width. The embedded geogrid area was 1.13 m². Data from the pullout tests are of particular significance for the assessment of the anchorage capacity in soil-reinforcement systems. This paper gives details for the test apparatus, testing procedure and discusses the test results.

¹ Centre for Geosynthetics Research, Information and Development, Civil Engineering, Carleton University, Ottawa, Canada.

² Geotechnical Research Centre, Faculty of Applied Science and Engineering, University of Western Ontario, London, Canada.

ANCHORAGE CAPACITY AND INTERFACE STRENGTH COEFFICIENTS

The anchorage capacity of a soil-reinforcement system resisting pullout may be expressed in terms of the soil-reinforcement interface strength as expressed by the interface cohesion and the interface friction angle (Jewell et al., 1984);

$$T_a = C_p + \sigma_n \tan \phi_p \tag{1}$$

where

- T_a = soil-reinforcement interface strength
- σ_n = normal stress on the reinforcement
- C_p = soil-reinforcement interface cohesion
- ϕ_p = soil-reinforcement interface friction angle

The interaction shear strength, therefore, can be determined from pullout tests by measuring the geogrid anchorage capacity at failure

$$T_a = R'_a / 2L_e B_e \tag{2}$$

where the factor 2 is attributed to the two interfaces between soil and reinforcement, and

- T_a = soil-reinforcement interaction strength
- L_e = embedded length of geogrid
- B_e = embedded width of geogrid
- R'_a = anchorage resistance at initiation of pullout failure

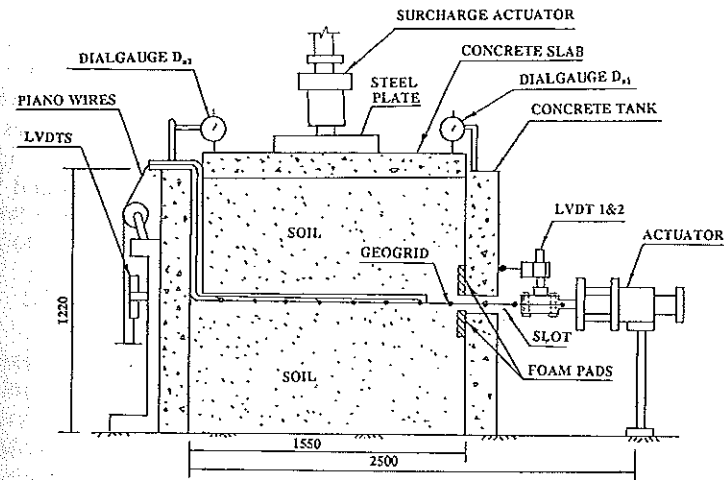
The interface strength parameters, C_p and ϕ_p , can be determined from Eq.(1) and the interaction strength is obtained from Eq.(2).

APPARATUS

A schematic diagram of the test apparatus is shown in Fig. 1. The test tank, with inside dimensions of 1.55 m by 0.9 m in plan and 1.22 m deep, was made by bolting together four reinforced concrete wall panels. The inside walls were lined with polished stainless steel sheets in order to reduce wall friction effects. A 0.22 m wide and 0.9 m long horizontal slot was cut at the mid-height of the front wall in order to pull the geogrid through. Foam pads were glued on both sides of the slot to prevent stress concentration and soil loss during pullout. The geogrid was gripped by metal jaws which were connected to the pullout actuator.

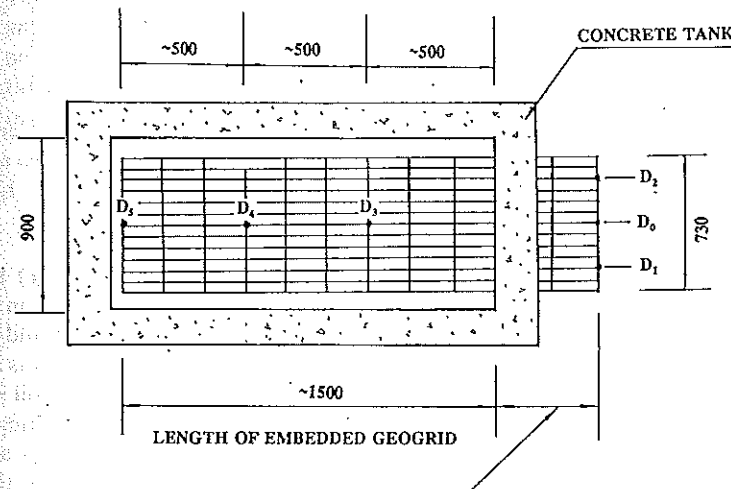
The test system consisted of an MTS function generator, a servo-hydraulic controller, an actuator assembly and a clamping mechanism for the geogrid. The pullout force was applied horizontally by a 100 kN capacity hydraulic actuator equipped with a load cell and an LVDT (linear voltage displacement transformer) to measure the pullout resistance and the geogrid displacement, respectively. The actuator was bolted to the reaction frame which in turn was anchored to the concrete

PULLOUT RESISTANCE



Note: All dimensions given in mm

a) SECTIONAL VIEW



Note: All dimensions given in mm

D = LOCATION OF LVDT POINTS

b) PLAN VIEW AT GEOGRID ELEVATION

Fig. 1 Pullout Test Apparatus

floor. The pullout rate was 1 mm/min in all tests. This rate has been adopted by other researchers and does not guarantee "drained" conditions for all soils, especially in clays (Ingold, 1983; Jewell et al., 1984 and Mowafy, 1986). This pullout rate was similar to the rate used by previous investigators (Mowafy, 1986; Ingold, 1983). The schematic diagram of the clamping device is shown in Fig. 2. Two pieces of stiff rubber were inserted between the steel jaws to prevent slippage of the geogrid during testing. Other gripping devices, such as metal clamps, "liquid" metal and "roller" jaws, were tried but some slippage did occur with these grips.

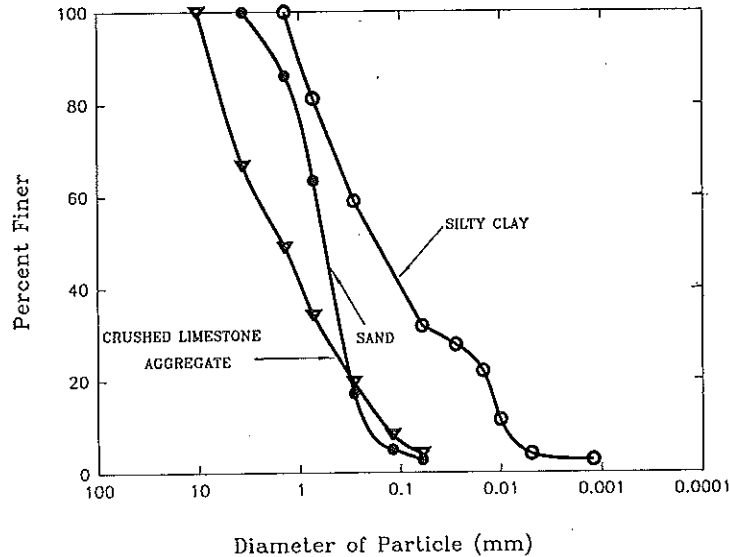


Fig. 2 Geogrid Clamping Assembly

Similar to the horizontal pullout system, the vertical (surcharge) loading system consisted of a hydraulic actuator equipped with a load cell and an LVDT controlled by the same MTS system. A steel plate, 230 mm in diameter and 80 mm thick, was attached to the lower end of the actuator ram. The surcharge was applied through a steel plate to a concrete slab which rested on the horizontal soil surface. The concrete slab was 150 mm thick and was considered to be rigid. Tilting of the concrete slab, if any, was monitored by two dial gauges, indicated as D_{n1} and D_{n2} in Fig. 1(a). These gauges were located on diagonally opposite corners of the slab.

In order to measure the geogrid elongation during a test, 0.1 mm diameter stainless steel wires (piano wire) were connected to cross-members of the embedded geogrid. These wires were connected to LVDT's located outside the tank. In order to minimize friction, the steel wires were fed through thin plastic tubes. The wires were kept tensioned by springs and the whole system functioned extremely well. This measuring system was used by other researchers with good results (Mowafy, 1986

and Palmeira and Milligan, 1989). Two additional LVDT's monitored the free-end displacement and any twist of the geogrid (Fig. 1b).

The data acquisition system consisted of a Hewlett Packard 9836 Instrument Controller with a 15 Mbyte hard disk subsystem, a Hewlett Packard 3497A Data Acquisition/Control Unit with 15 slots. The computer controlled the entire testing procedure and collected data at predetermined time intervals.

Several trial tests were carried out. The results showed satisfactory repeatability. Twisting of the geogrid and tilting of the slab were negligible.

SOIL PROPERTIES AND GEOGRID SPECIFICATIONS

Three soils were used in this investigation, a medium coarse sand, a well-graded lime-stone aggregate and a reconstituted clay. The clay was reconstituted from a dry silty clay powder used to manufacture clay bricks. It was compacted to 90% of Modified Proctor density and optimum moisture content. The choice of the testing soils were based on the following considerations:

1. Current specifications for reinforced soil structures generally require the use of granular backfill materials; sand is most commonly used whereas crushed rock aggregate has the best mechanical properties.
2. The use of a cohesive soil as backfill material could have economic advantages and, therefore, its interaction behaviour should be studied. It should be noted that the clay material was only partially saturated and drainage conditions in the vicinity of the geogrid are not known.

The grain size distributions of these soils are given in Fig. 3. The optimum moisture content and the maximum dry unit weight of the soils as well as the plastic limit and the plasticity index for the silty clay are summarized in Table 1.

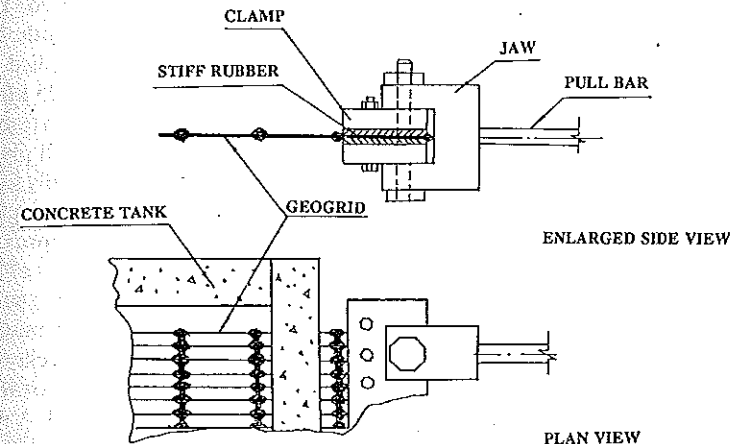


Fig. 3 Particle Size Distribution of Test Soils

Table 1 Properties of Test Soils.

SYSTEM	γ kN/m ³	w %	c kPa	ϕ °	PL %	PI	γ_0 kN/m ³	ω_0 %	Relative Compaction, %
Gravel	19.0	1.5	0	40°	-	-	21.6	6.8	88
Sand	17.6	3.5	0	32°	-	-	19.2	11	92
Clay	18.0	11.5	7.45	16°	15.6	8.4	21.3	8.7	85
Sand/Clay	-	-	2.95	26°	-	-	-	-	-

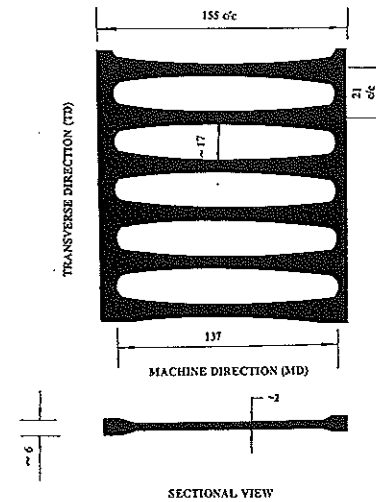
Note:

- γ = soil dry unit weight
- ω = soil moisture content
- c = soil cohesion
- ϕ = soil friction angle
- PL = plastic limit
- PI = plasticity index
- γ_0 = Modified Proctor density of soil
- ω_0 = optimum moisture content of soil

The shear strength properties of the three soils were determined by direct shear tests. Due to the large size of the soil particles a large shear box was used. The box had dimensions of 550 mm in length, 210 mm in width and 380 mm in depth. Normal stresses were applied to the top of the box by a dead load system. The applied normal stresses were in the same order as those used in the pullout tests (15 to 25 kPa). The soils were hand tamped into the box at densities and moisture contents corresponding to 90% Modified Proctor. This specification is generally adopted for soil placement in the field. It should be kept in mind that the reconstituted clay was not fully saturated when compacted. Shearing was commenced as soon as vertical settlement had ceased under a given surcharge load. For the clay specimens this occurred at approximately two hours at low normal stresses and about three hours at a normal stress of 25 kPa. The granular soil specimens could be sheared within a few minutes after the surcharge was applied. The shear rate for the clay specimens was set at 0.006 mm/min. Shang (1989) has shown from the results of undrained triaxial tests on the same clay that no excess porewater pressures were developed when sheared at this rate. For the sand and stone aggregate specimens a shear rate of 0.3 mm/min was employed. A series of tests was also performed in which the bottom half of the shear box was filled with clay and the top half with sand in order to obtain the interface strength parameters

for the pullout tests where the geogrid was sandwiched between a clay and sand layer as explained later. The same shear rate as for the clay specimens was adopted. The shear strength properties for the test soils are also given in Table 1.

The geogrid (Tensar UX1600) was a uniaxial polymer geogrid (Fig. 4). The specifications of the grid are summarized in Table 2. In this investigation, a series of tension tests was performed to determine the tensile modulus and deformation properties of two specimens (i.e., 35 and 17 longitudinal ribs, respectively) at a rate of 1 mm/min.



Note: All dimensions given in mm

Fig. 4 Geogrid (TENSAR UX 1600)

For the tension tests, the pullout test apparatus was modified as shown in Fig. 5. A second pair of clamps was attached to the back wall of the test tank to hold the geogrid in place. The tensile force was applied horizontally by the pullout actuator at a rate of 1 mm/min. The tensile force and the corresponding geogrid deformation were recorded.

Two geogrid specimens were tested in tension. The first specimen had the same dimension as the meshes used in the pullout tests, i.e., 1.55 m long and 0.73 m wide. The second specimen had the same length of 1.55 m but the width was reduced to 0.38 m in order to check if a variation in width had any influence on the stress-strain relationship.

The tensile modulus of the geogrid was defined as

$$E_g = \Delta T / \Delta \epsilon \tag{3}$$

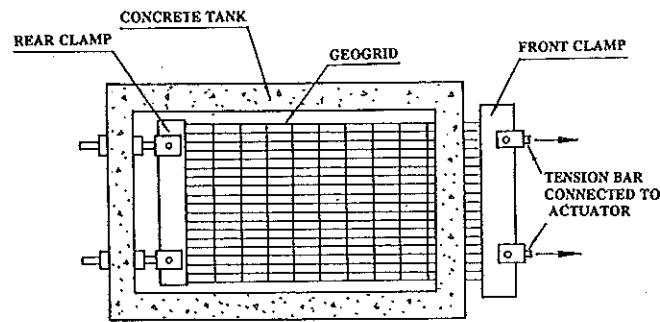


Fig. 5 Tension Test Rig for Geogrid

where

ΔT = increment of tensile force per unit width of geogrid, in kN/m
 $\Delta \epsilon$ = corresponding increment of average strain in the geogrid

Unit tensile force against geogrid strain for the two specimens are plotted in Fig. 6. The two relationships are in good agreement. At small initial strain, the initial tangent modulus, as shown in Fig. 6, had a value of

$$E_{go} = 1732.8 \text{ kN/m}$$

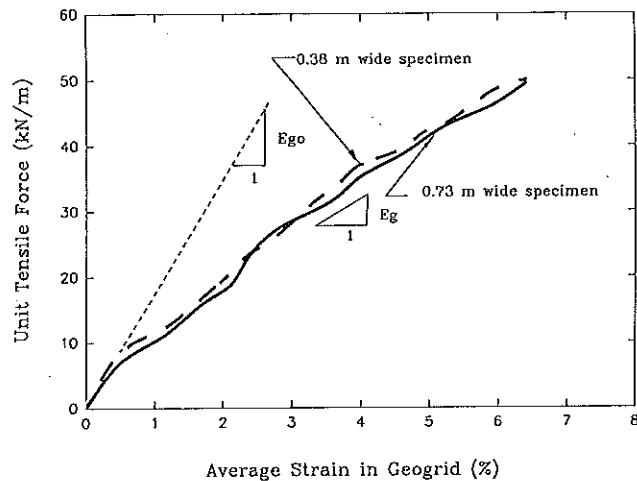


Fig. 6 Tensile Force vs Geogrid Strain Response

This value is about 40% lower than that given by the manufacturer (Table 2). Over a strain range from 2% to 6%, the tensile modulus remained fairly constant and had a value of

Table 2 Properties of Tensar Geogrid (UX1600).

PROPERTY	MEASURED	MANUFACTURER PROVIDED ^a
Material		High density polyethylene
Dimensions		Roll length 30 m Roll width 1 m Roll weight 34 kg
Rstrand & Bearing member		Apertures:
$l^b = 155 \text{ mm}$		MC ^c 137 mm
$s^d = 21 \text{ mm}$		TD ^e 17 mm
		open area 60%
Junction thickness	$t^f = 6 \text{ mm}$	6 mm
Modulus		
Initial tensile modulus, E_{go}	1732.8 kN/m	2918 kN/m
Tensile modulus (2 to 6%)	688.1 kN/m	1022 kN/m
Peak strength	N.A. ^g	129.5 kN/m
Long-term design load		43.8 kN/m
Testing condition		
Specimen sizes	(a) 1.55 m, length 0.73 m, width (b) 1.55 m, length 0.38 m, width	single strand
Tension rate	1 mm/min	102 mm/min

^aTensar Co. Product Catalogue, 1987

^bStrand length (adjacent bearing member spacing), Fig. 4

^cAlong roll length

^dAdjacent strand spacing, Fig. 4

^eAcross roll length

^fBearing member thickness, Fig. 4

^gActuator stroke limit

$$E_g = 688.1 \text{ kN/m}$$

This value is about 30% lower than that obtained from a single strand, as given by the manufacturer (Table 2).

The strain rate dependency of polyethylene is well known. It has been reported that as the strain rate decreased from 100%/min to 1%/min, the secant modulus decreases in the order of 40% and the corresponding tensile strength decreased by 60% for polyethylene monofil (Zanten 1986). As already mentioned, the elongation rate was 1 mm/min for the tension tests conducted in this investigation, and 102 mm/min for tests by the manufacturer. Thus the difference in tensile moduli as found from the experiments in relation to those reported by the manufacturer can be attributed to two main differences: (1) single strand versus multistrand grid and (2) difference in strain rates.

The experimental data of the tension-deformation behaviour are summarized in Table 2, together with data provided by the manufacturer.

SOIL-REINFORCEMENT SYSTEMS

Four soil-geogrid systems were investigated. All soils were compacted in layers in the test tank at 90% of Modified Proctor density as in the direct shear tests.

1. **Sand-system.** The geogrid was embedded in the compacted sand deposit having a dry unit weight of 17.6 kN/m^3 and a moisture content of 3.5%.
2. **Clay-system.** The compacted silty clay had a dry unit weight of 18.0 kN/m^3 and a moisture content of 11.5%.
3. **Sand-clay-system.** The lower half of the test tank was compacted with silty clay and the upper half with compacted sand. The unit weights and moisture contents of the two soils were the same as those in the sand-system and in the clay-system. This mixed system was to simulate a field condition where the geogrid was placed on a clay base overlain by a granular embankment.
4. **Aggregate-system.** The geogrid was embedded in a compacted crushed limestone aggregate having a dry unit weight of 19.0 kN/m^3 and a moisture content of 1.5%.

The minimum thickness of the soil layers below and above the reinforcement was 0.6 m. For the clay-system, the pullout tests were carried out after the settlement had ceased under the applied surcharge load. Due to the low normal stresses, vertical compression was quite small. A summary of the physical properties of the soils are also given in Table 1.

Three pullout tests were carried out for surcharges of 0, 5 and 10 kN, respectively. The surcharge was kept constant in each test. The normal stress intensity on the reinforcement plane was governed by the tensile strength of the geogrid. As the normal stress increased to a critical level, tensile failure would occur. Several trial

tests were conducted in order to determine the maximum allowable surcharge load without causing tensile failure of the geogrid.

The effective normal stress on the reinforcement plane in each reinforcement system was estimated from the weight of the soil mass located above the reinforcement plane, the weight of the concrete slab and the surcharge load applied by the hydraulic ram. Rabbaa (1981) determined the influence of side friction in tanks on vertical stress distribution with depth. Based on his results the reduction of the normal stress on the reinforcement plane, due to wall friction, was in the order of 5% to 8% near the walls. The influence of wall friction, therefore, was neglected considering the relatively large plan area of the tank ($0.9 \text{ m} \times 1.55 \text{ m}$).

TEST PROCEDURE

All geogrid specimens were cut to the same size, i.e., 1.55 m long (10 transverse members) and 0.73 m wide (35 longitudinal ribs). Each soil, having the appropriate moisture content, as listed in Table 1, was deposited in layers in the tank and then compacted. The geogrid was placed on the soil surface when the compacted soil had reached the mid-height of the tank. Thin piano wires were then firmly attached with special clamps at the designated geogrid transverse members, threaded through plastic tubes and extended to the outside of the tank and connected to LVDT 3, 4 and 5 (Figs. 1a and 1b). The placement and compaction of the soil was then continued until the tank was filled. In-place soil density was measured by a nuclear density meter. The deviation of in-place densities in the three tests for each soil-reinforcement system was within $\pm 2.5\%$. The concrete slab was put in place after the soil surface had been carefully levelled in order to ensure an even and uniform contact. Then the surcharge was applied and the settlement was recorded. The last phase of test preparation consisted of installing and connecting monitoring devices and performing an operational check on all instrumentation and actuators.

A complete set of the test data included the pullout resistance (in kN), the free end displacement of the geogrid (in mm), the surcharge load (in kN), the vertical displacement (in mm) and the geogrid displacements at five locations (in mm), D_1, D_2, D_3, D_4, D_5 (Fig. 1b). Each test lasted about two hours.

The pullout test was terminated when either of the two situations occurred:

1. The pullout displacement reached a value of 100 mm. This displacement was sufficient in all soil system to reach a residual value for pullout resistance. A check of the geogrid specimens after a test was done for any physical damage and to verify that the grid was not plastically deformed.
2. The pullout force reached the capacity of the actuator. The pullout load actuator was set to shut off when its capacity was reached. This occurred twice in the crushed stone aggregate system under high surcharge loads.

OBSERVATION

The pullout force applied by the actuator at the free end of the geogrid is resisted by the shear stresses mobilized along the embedded part of the geogrid. This stress transfer mechanism can be visualized in several stages as indicated in Fig. 7.

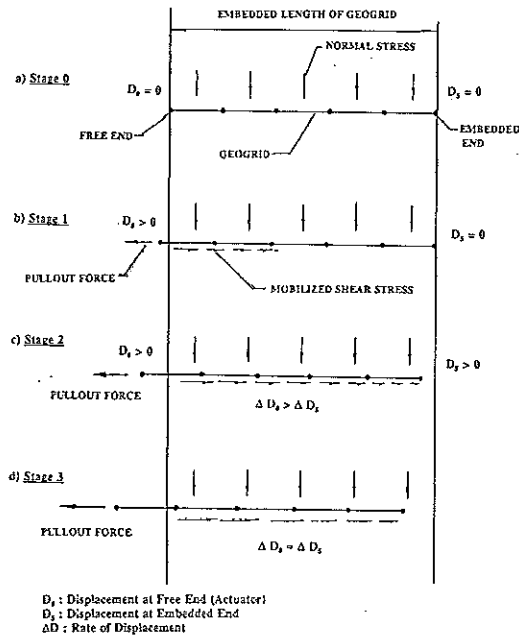


Fig. 7 Mobilization of Pullout Resistance

Stage 0. No pullout force is applied yet to the grid. The only stresses acting on the mesh are the vertical or normal stresses from the soil overburden plus the applied surcharge load. At this stage there are no shear stresses mobilized and no grid displacement has occurred.

Stage 1. The applied force causes tensile strains in the mesh. The tensile force is resisted by shear stresses mobilized at the soil/geogrid interface. During this stage shear stresses are mobilized along the free end part of the geogrid. The free end of the mesh is displaced ($D_0 > 0$) but the embedded end has not moved yet ($D_5 = 0$).

Stage 2. As the free end of the geogrid is further displaced the pullout resistance increases. Eventually the embedded end of the geogrids is also displaced but at a smaller rate as the front end. In other words the geogrid is stretched as indicated by the relative displacement of the two ends ($D_0 - D_5 > 0$). The unit pullout force, that is

the measured pullout force divided by the width of the geogrid when the embedded end starts to be displaced is termed the anchorage capacity, R'_a , of a reinforcement. This definition has been adopted by Jones (1985).

The anchorage capacity, R'_a , of the geogrid is defined in Eq. (5) (in kN/m).

The anchorage capacity is not necessarily the maximum pullout resistance obtained in a pullout test. This is shown in Fig. 8 for the different soil systems. After the anchorage capacity is reached, the embedded end of the geogrid starts to be pulled through the soil and additional shear stresses are mobilized. The increase in pullout force, after the anchorage capacity was reached, is due to slipping of the grid relative to the adjacent soil. The increase in strain after the whole geogrid starts to be pulled out was explained by Jones (1985). He attributed this increase to mobilization of the bearing capacity of the soil caused by the transverse members of the embedded geogrid. Also in order for the geogrid to be pulled through the soil, the particles interlocking with the grid apertures have to be dislodged or dragged along, and consequently mobilizing more soil strength in the vicinity of the moving geogrid. The monitoring of the displacement of the embedded end of the grid is essential in order to determine when the anchorage capacity is reached or, in other words, when the whole geogrid starts to move through the soil mass. The shear stress distribution along the geogrid is not uniform as indicated by the non-uniform displacement measured at several points on the grid. This aspect will be discussed later with reference to Fig. 9.

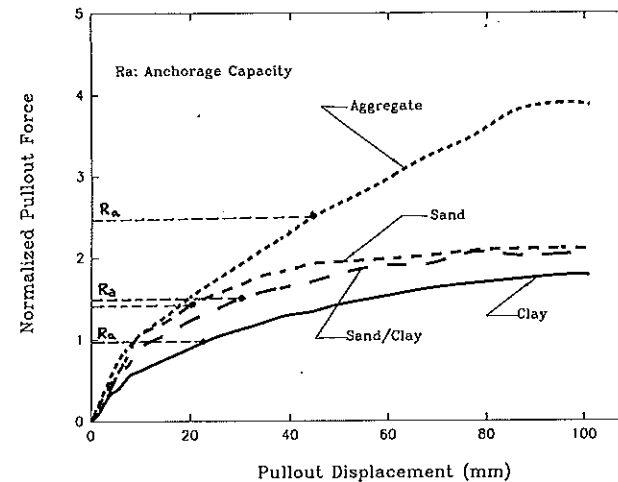


Fig. 8 Normalized Pullout Resistance vs Geogrid Displacement

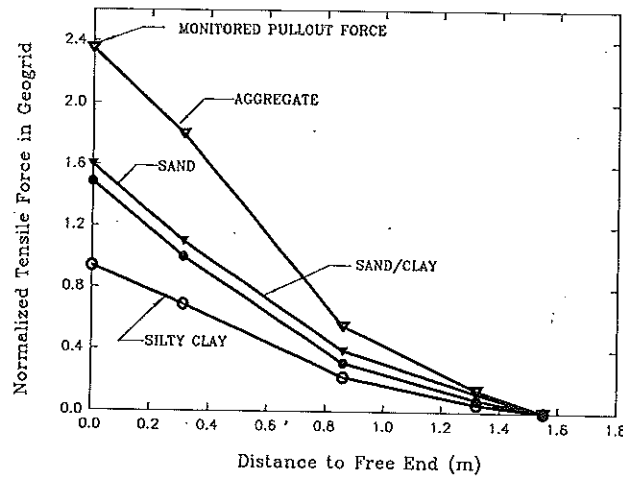


Fig. 9 Tensile Force Distribution along Geogrid

Stage 3. As the geogrid is further pulled through the soil, a maximum pullout resistance is reached and the two ends of the grid are displaced at the same rate, as shown in Fig. 7d. The average strain and the pullout resistance in the geogrid remain constant.

RESULTS AND DISCUSSION

The relationship between the normal stress on the embedded geogrid and the pullout force is linear for the limited normal stress range tested. The normalized pullout force, therefore, can be defined as the pullout force applied by the actuator divided by the surcharge load acting on the reinforcement, or

$$R = R' / (\sigma_n L_e) \tag{4}$$

where R' is pullout force per unit width of geogrid, σ_n is the normal stress, and L_e is the length of the embedded geogrid. The anchorage capacity is then defined as the normalized pullout force at initiation of displacement of the embedded grid end (Jones, 1985),

$$R_a = R'_a / (\sigma_n L_e) \tag{5}$$

where R_a is the anchorage capacity of the reinforcement system in terms of normalized pullout force, and R'_a is the measured anchorage capacity of a particular geogrid.

The anchorage capacities calculated from the applied normal stresses for each soil reinforcement system are quite consistent, as shown in Table 3. The average value of R_a for a particular system, therefore, is taken as the anchorage capacity for this system. Table 3 also gives the values of the maximum pullout resistance, R_m , for each system as obtained from pullout tests and in the last column the ratio of R_a/R_m is presented.

Table 3 Summary of Anchorage Capacity

System	σ_n kPa	R'_a kN/m	R_a	R_a Ave.	R'_m kN/m	R_m	R_m Ave.	R_a/R_m
Sand	12.1	20.9	1.40	1.48	30.7	2.04	2.02	0.73
	16.3	24.7	1.47		41.6	2.06		
	20.4	33.2	1.57		49.8	1.97		
Clay	13.3	17.5	1.06	0.96	35.8	2.17	1.85	0.52
	17.4	20.0	0.93		39.3	1.82		
	21.6	24.2	0.90		41.8	1.56		
Crushed Aggregate	12.9	36.7	2.30		63.7	3.98		0.58
Sand/Clay	12.1	25.0	1.67	1.52	35.2	2.34	2.16	0.70
	16.3	29.9	1.47		42.8	2.12		
	20.4	35.9	1.42		50.9	2.01		

Note:
 σ_n : Normal stress on reinforcement plane
 R'_a : Anchorage resistance
 R_a : Anchorage capacity (normalized anchorage resistance)
 $R_a(Ave.)$: Average of anchorage capacities from the three pullout tests
 R'_m : Maximum pullout resistance
 R_m : Normalized maximum pullout resistance
 $R_m(Ave.)$: Average of normalized maximum pullout forces from the three pullout tests.

Figure 8 shows the relationships between the normalized pullout resistance and the free end displacement of the geogrid for the four soil-reinforcement systems. This figure shows clearly an increase of pullout force beyond the anchorage capacity. However, after R_a is exceeded, a small increase in the pullout force will induce a relatively large displacement due to slippage occurring between the soil and the geogrid. The amount of increase in pullout force beyond the anchorage capacity is

largely dependent on the specific reinforcement system, as shown in Fig. 8. The residual pullout resistance is reached when under continued grid displacement no further resistance is mobilized. At this stage (stage 3 of Fig. 7d) the rate of displacement of the two ends of the geogrid are the same.

The average strain within the geogrid can be estimated from the difference of the relative displacements between any two measuring points on the embedded geogrid

$$\epsilon_i = (D_i - D_{i+1}) / \Delta L_i \quad (6)$$

where

- ϵ_i = average strain from the i^{th} grid point to the $(i + 1)^{\text{th}}$ grid point
- D_i = displacement of the i^{th} grid point
- D_{i+1} = displacement of the $(i + 1)^{\text{th}}$ grid point
- ΔL_i = gauge length, i.e., distance over which grid elongation is monitored.

The average tensile force over a section of an embedded geogrid, therefore, can be estimated from

$$F_i = E_g \epsilon_i = 1,2,3 \quad (7)$$

where F_i is the tensile force in the geogrid; E_g is the modulus of the geogrid determined from the tension test results given in Fig. 6. It should be noted that the tensile modulus is a function of the average strain in the geogrid, as shown in Fig. 6. Similar to the normalized pullout resistance, the tensile force obtained from Eq. (6) can be normalized because of the linear relationship between the effective normal stress and the tensile force in the geogrid.

$$F_i = F'_i / (\sigma'_n L_e) \quad (8)$$

where

- F'_i = normalized tensile force in geogrid
- σ'_n = effective normal stress; and
- L_e = Length of the embedded geogrid

The normalized tensile forces obtained from Eq. (7), at the stage when the anchorage capacity was reached for a particular soil/reinforcement system, are plotted against the distance to the free end of the geogrid in Fig. 9.

An understanding of tensile force distribution over the embedded grid length is of importance for the design of a reinforced soil structure incorporating geogrids. Currently a linear tensile force distribution is normally assumed for design purposes (Jones, 1985). A pullout test in which the strains are monitored in the geogrid will clarify some aspects of the distribution. As shown in Fig. 9 the pullout test results indicate that the tensile force distribution over the grid length is not linear. The tensile force is highest at the leading end of the embedded geogrid with a rapid decrease towards the rear part. This can be attributed to the relatively low stiffness of

the geogrid which reduces the efficiency of load transfer in the soil, as indicated by Ingold (1983). It should be pointed out that stress concentrations at the pullout slot were minimized as much as possible by adding compressible foam pads around this opening (Fig. 1a).

The pullout tests in the sand system were conducted at normal stresses of 12.1, 16.3 and 20.4 kPa, respectively. The corresponding anchorage capacity and maximum pullout resistance are given in Table 3. The average anchorage capacity of the sand-system is 1.48 in terms of normalized pullout resistance. As shown in Fig. 10, the relationship between the normal stress and the geogrid-soil interaction strength was taken to be linear over the narrow normal stress range used in this study. An interface friction angle of 36° was obtained.

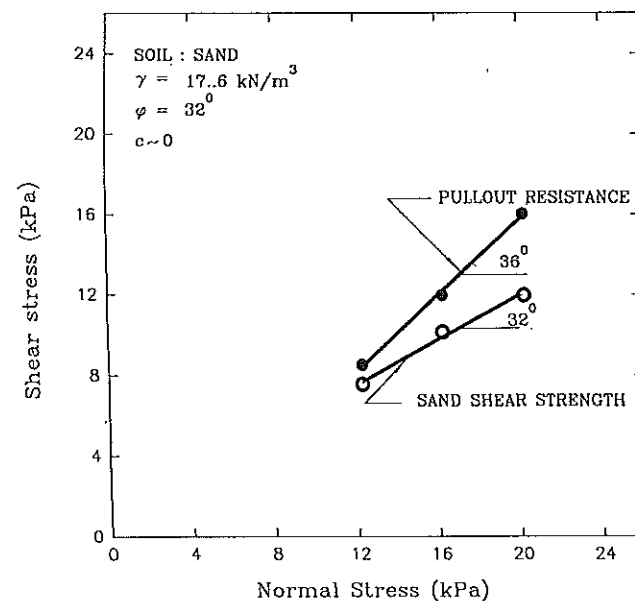


Fig. 10 Shear Strength and Pullout Resistance-Coarse Sand

The tests in the clay-system were conducted at normal stresses of 13.3, 17.4 and 21.6 kPa, respectively. The average anchorage capacity of the clay-system was found to be 0.96 in terms of normalized pullout resistance (Table 3). The low anchorage capacity may be due to the fine soil particles of the silty clay providing little interlock with the geogrid apertures.

The linear relationship between the normal stress and the soil-geogrid interface strength yielded an interface friction angle of 18° and an interface cohesion of 2.5 kPa

(Fig. 11). It should be noted that the interface friction angle is close to the soil friction angle, i.e., 16°. On the other hand, the interface cohesion is significantly lower than the soil cohesion. The friction angle and adhesion between the polyethylene sheet and the silty clay were measured as 9° and 0, respectively. The small cohesive coefficient is obviously due to the smooth surface of the polyethylene material.

In the sand/clay-system the normal stress levels were the same as those for the sand-system. The average anchorage capacity of the sand/clay-system is 1.52 in terms of normalized pullout resistance (Table 3). The effective normal stress and soil-geogrid interface strength relationship yielded a soil-geogrid interface friction angle of 33°, compared to the sand/clay interface friction angle of 26°. The soil-geogrid interface cohesion was found to be 3.0 kPa (Fig. 12), similar to the value of the sand/clay interface cohesion (2.9 kPa).

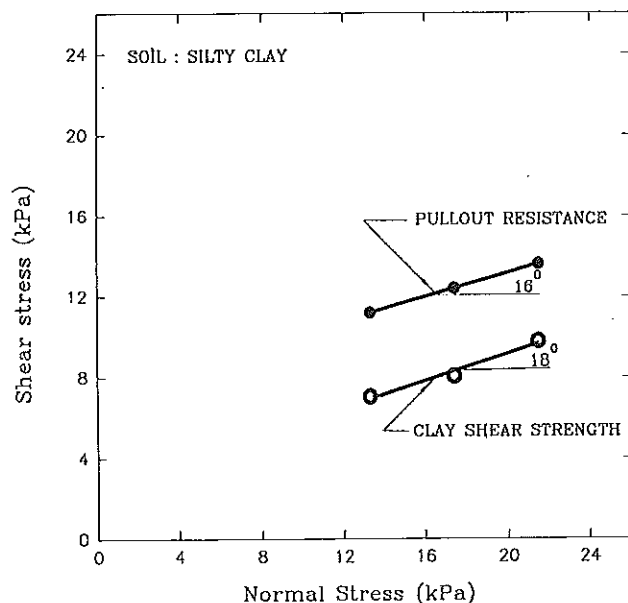


Fig. 11 Shear Strength and Pullout Resistance-Silty Clay

As mentioned before, two of the three pullout tests in the limestone aggregate-system were terminated when the actuator reached full capacity. The maximum pullout resistance therefore, could not be obtained. In spite of this, the crushed stone aggregate exhibited the best pullout resistance of all soils. At a normal stress of 12.9 kPa, the anchorage resistance was 36.7 kN/m, giving an anchorage capacity of 2.30 in terms of normalized pullout resistance (Table 3), higher than the corresponding values of the other systems. This high value is obviously due to the good interlock of

PULLOUT RESISTANCE

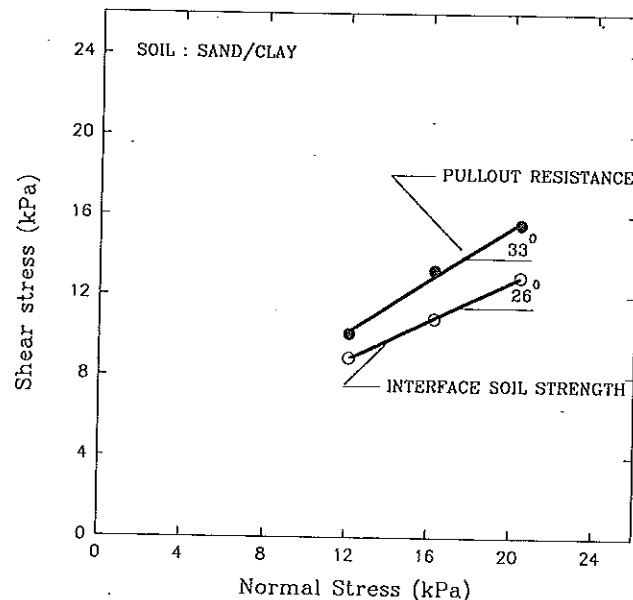


Fig. 12 Shear Strength and Pullout Resistance-Coarse Sand/Silty Clay Interface

the soil particles with the apertures of the grid. The opening to grain size ratio is defined as the ratio of the smallest grid opening to the average soil particle size. It was proposed that the optimum ratio should be in the order of 3.5 (Sarsby, 1985). The ratio in the aggregate-system was 4.5.

Table 4 summarizes the soil-geogrid interface strength parameters for the three soil-reinforcement systems.

In summary, the features of an embedded geogrid under a pullout force include the nonuniform tensile force distribution over the embedded length and the attainment of the anchorage capacity (as defined earlier) before the maximum pullout resistance was reached. Both of these features should be investigated further in order to determine the performance of embedded geogrids in a soil-reinforcement system.

CONCLUSIONS

This paper presents the results of a laboratory test program using a large pullout test facility. The following conclusions can be drawn from the study.

Table 4 Soil-Geogrid Interface Properties and Strength Coefficients.

	c kPa	ϕ	c_p kPa	ϕ_p
Sand-system	0	32°	0	36°
Clay-system	7.45	16°	2.5	18°
Sand-clay-system	2.92	26°	3.0	33°

Note:

c = soil cohesion

ϕ = soil friction angle

c_p = soil-geogrid interface cohesion

ϕ_p = soil-geogrid interface friction angle

1. The large test facility described in this study has been found effective to investigate the anchorage capacity of a meshlike geogrid. The facility has adequate size and capacity to test representative grid specimens in soils compacted to field densities and moisture contents.
2. The initiation of pullout failure in a soil-geogrid system occurs when the embedded end of the geogrid starts to move (Jones, 1985). The corresponding resistance is defined as the anchorage capacity of the geogrid. In all cases the resistance increases with further geogrid displacement until an ultimate or residual resistance value is reached.
3. A linear relationship between the normal stress and the soil-geogrid bond strength existed in all tested soil-reinforcement systems over the narrow normal stress range used in this study. The aggregate-system had the greatest anchorage resistance. This is attributed in part to the good interlock between grid apertures and soil particles.
4. The tensile force distribution over the embedded part of the geogrid is nonlinear. Both the anchorage capacity and the tensile strength of the reinforcement should be considered in order to avoid pullout failure and material failure in a soil-reinforcement system.

REFERENCES

- INGOLD, T.S. (1983). Laboratory Pullout Testing of Geogrid Reinforcement in Sand. *Geotechnical Testing Journal*, Vol. 6, No. 3, pp. 101-111.
- JEWELL, R.A., MILIGAN, G.W.E., SARSBY, R.W. and DUBOIS, D.D. (1984). Interaction Between Soils and Grids. *Polymer Grid Reinforcement in Civil Engineering*, Thomas Telford, pp. 18-30.
- JONES, C.J.F.P. (1985). *Earth Reinforcement and Soil structures*, Butterworth and Co. Ltd., England.
- HOWAFY, Y.M. (1986). Analysis of Grid Reinforced Earth Structures, Ph.D. Thesis, Carleton University, Ottawa, Canada.
- PALMEIRA, E.M. and MILLIGAN, G.W.E. (1990). Large Scale Pullout Tests on Geotextiles and Geogrids. *Proc. 4th Int. Conference on Geotextiles, Geomembranes and Related Products*, The Hague, V. 2, pp. 743-746.
- RABBAA, S.A.A. (1981). Interference Between Rigid Strip Foundations Resting on Cohesionless Soils. Ph.D. Thesis, Department of Civil Engineering, Carleton University, Ottawa, p. 318.
- SARSBY, R.W. (1985). The Influence of Aperture Size/Particle Size on the Efficiency of Grid Reinforcement, *Proc. 2nd Canadian Symp. on Geotextile and Geomembranes*, Edmonton, Canada, pp. 7-12.
- SHANG, Q. (1989). Pullout Resistance of Geogrids Determined in a Large Test Facility. M. Eng. Thesis, Department of Civil Engineering, Carleton University, Canada, p. 115.
- TENSAR CO. (1987). Product Catalogue, 1210 Citizens Parkway, Morrow, GA 30260, U.S.A.
- ZANTEN, R.V.V. (Ed.) (1986). *Geotextiles and Geomembranes in Civil Engineering*, A.A. Balkema Publishers, pp. 119-120.